Journal of Inorganic and Organometallic Polymers and Materials (2020) 30:1898–1906
https://doi.org/10.1007/s10904-019-01320-y

Structural and Optical Properties of $Cd_{1-x}Mn_xFe_2O_4$/PMMA Nanocomposites

Zein K. Heiba[1,5] · Mohamed Bakr Mohamed[2,5] · Nasser Y. Mostafa[3] · A. M. El-Naggar[4,5]

Received: 15 August 2019 / Accepted: 9 September 2019 / Published online: 16 September 2019

Abstract
$Cd_{1-x}Mn_xFe_2O_4$/PMMA nanocomposites are prepared using hydrothermal and casting procedures. Rietveld analysis is performed for $Cd_{1-x}Mn_xFe_2O_4$ (x = 0, 0.3, 0.5, 0.7) nano ferrite. X-ray diffraction and Fourier transform infrared are used to examine the homogenous distribution of $Cd_{1-x}Mn_xFe_2O_4$ throughout PMMA matrix. The influence of nano ferrite on the absorbance, transmittance and refractive index for all samples are examined utilizing UV–Vis spectrophotometer technique. The direct energy gap and other optical parameters of nanocomposite samples are changed depending on the amount of manganese doped Cd-ferrite. All nanocomposite samples display four sub-emissions in UV and visible regions.

Keywords Nano ferrite · PMMA · Optical · Structural · Nanocomposites

1 Introduction

Polymer nanocomposites prepared by incorporating a small amount of inorganic nanoparticles into a polymer matrix, merging the characteristics of both organic and inorganic materials [1, 2]. Many properties of polymer such as refraction index and transmittance can be tuned by changing the ratio between inorganic and organic components [3]. Furthermore, polymer nanocomposites with new properties allowed them to be used in several potential applications such as optics, electronics, sensors and biological approaches [4].

Poly (methyl methacrylate) (PMMA) is among the well-tested group of polymers which gained unlimited interest in many industrial applications because of its promising optical characteristics, amorphous nature, high transparency in the visible region, low refractive index, scratch resistance, low cost, non toxicity and simple synthesis [5]. PMMA has both hydrophobic (methylene) and a hydrophilic (carbonyl) group in every monomeric unit [6].

Several inorganic materials have been inserted inside PMMA to introduce a photoluminescent characteristic in polymer [7].

Spinel ferrite nanoparticles with a general formula AFe_2O_4 (A is divalent ions) are widely used in several fields [8]. The properties of nano ferrite can be modified by altering the synthesis methods [9], doing elements [10] or annealing temperature [11]. $MnFe_2O_4$ ferrite has a cubic structure with space group Fd-3m which has been extensively used in the biological field for instance magnetic hyperthermia agent, MRI contrast agent and targeted drug delivery etc… [12]. Around 80% of nano $MnFe_2O_4$ belongs to a normal spinel structure [13]. Nano $CdFe_2O_4$ also has a normal spinel cubic structure with a narrow band gap [14]. Additionally, the optical band gap of ferrite affected by kind of dopant element, for example, the band gap of NiZnCo-ferrite is increased as it doped with La ion, but it reduced as it doped with Gd ion [15].

Bisen et al. [16] found that the band structure of PMMA can be modified as it doped with a small amount

✉ Mohamed Bakr Mohamed
mbm1977@yahoo.com

1 X-ray Unit, Faculty of Science, Ain Shams University, Cairo, Egypt

2 Physics Department, Faculty of Science, Taibah University, Al-Madina al Munawarah, Saudi Arabia

3 Chemistry Department, Faculty of Science, Suez Canal University, Ismailia 41522, Egypt

4 Research Chair of Exploitation of Renewable Energy Applications in Saudi Arabia, Physics & Astronomy Department, College of Science, King Saud University, P.O. Box 2455, Riyadh 11451, Saudi Arabia

5 Physics Department, Faculty of Science, Ain Shams University, Abbasia, Cairo 11566, Egypt

of coumarone. Khursheed et al. [17] found that the thermal stability and glass transition temperature of PMMA are improved as it doped with $KCaVO_4:Sm^{3+}$. Moreover, ZnSe:Mn/ZnS/PMMA nanocomposite revealed a high transmittance in the visible spectral range, an extremely bright orange fluorescence and an enhancement in refractive index [18]. Bai et al. [19] reported that the luminescence properties of PMMA are enhanced when it doped with 11 wt% of $Eu_2(PBT)_3(NO_3)_3$. Khursheed et al. [17] revealed that the glass transition temperature of PMMA did not affect as it doped with $Sr_3B_2O_6:Dy^{3+}$ but its thermal stability increased. Padalia et al. [20] found that the glass transition temperature of PMMA reduced as it is doped with Fe_3O_4:Ce. Ding et al. [21] revealed that the thermal stability of Fe_3O_4/polyimide nanocomposites improved while the band gap reduced with increasing the Fe_3O_4 loading amount.

The investigation of different optical dispersion parameters of ferrite loaded in PMMA matrix is rarely investigated in the literature. Therefore, the aims of the present work is prepared $Cd_{1-x}Mn_xFe_2O_4$/PMMA nanocomposites, then, investigate the structural properties of the obtained nanocomposites using Fourier transform infrared and X-ray diffraction techniques. Finally, the effect of ferrite doping on absorption, transmittance, refractive index, other optical behavior and photoemission properties of PMMA loaded with nano $Cd_{1-x}Mn_xFe_2O_4$ ferrite is studied using UV–Vis. Spectrophotometer and photoluminescence spectroscopes.

2 Experimental

Nano $Cd_{1-x}Mn_xFe_2O_4$ ($x=0$, 0.3, 0.5, 0.7) ferrite was prepared by hydrothermal procedure; a stoichiometric amount of ferric, manganese and cadmium chlorides were dissolved in distilled water using a magnetic stirrer. The pH of the solution was modified to be 12 by adding NaOH solution before transferred it to a Teflon-lined autoclave. The autoclave was put inside furnace and heated at 180 °C for 20 h. The formed samples were got by washing and filtering the solutions several times using distilled water and anhydrous ethanol and then dried at 50 °C in a vacuum. The composites PMMA/$Cd_{1-x}Mn_xFe_2O_4$ films were formed by solution casting procedure. Powdered PMMA was dissolved in chloroform to obtain a clear solution. Then $Cd_{1-x}Mn_xFe_2O_4$ was added to the above solution and sonicated for 30 min in weight ratio x (0.5 wt%) with regard to PMMA according to the next relation:

$$x(\text{wt}\%) = \frac{w_f}{w_p + w_f} \times 100$$

where w_f and w_p are the weights of ferrite and PMMA respectively.

Then the solutions were casted in Petri dishes and left in air for 3 days. X-ray diffraction was gathered in step-scan mode ($2\theta = 10$–80) using Panalytical diffractometer (X'pert MPD, Cu-K_α). The instrumental broadening was corrected by LaB_6 standard. The crystal structure and microstructure were evaluated using Rietveld profile procedure applying MAUD software [22]. UV spectra of different samples were carried out by UV–vis. Spectrophotometer (Model Tomos UV-1800). Photoluminescence (PL) data were recorded by a luminescence spectrophotometer (RF-1501 SHIMADZU, Ltd.). Fourier transform infrared (FTIR) spectroscopy (Bruker Tensor 27 FTIR Spectrometer) was measured in 400–4000 cm^{-1} range.

3 Results and Discussion

3.1 X-ray Diffraction and Structural Analysis

Figure 1a reveals the phase analysis of X-ray diffraction patterns (XRD) of the $Cd_{1-x}Mn_xFe_2O_4$ samples. Search match analysis indicated that all samples have spinel structure with some minors of Fe_2O_3 phase for some values of x. Rietveld analysis investigation is carried out by MAUD software [22]; Table 1 provides the refined structural parameters and Fig. 1 illustrates the XRD pattern fitting for samples with $x=0$ and 0.3. During the Rietveld refinement, it is found that Cd^{2+} cations prefer to reside in 8b tetrahedral positions, while Mn^{2+} cations preferred to occupy 16d octahedral positions. Inspecting Table 1, it is found that the lattice parameter (a) and oxygen position parameter (u) decreased, while the crystallite size increased as the manganese doped amount increased. The decrease in the cell parameter is attributed to the difference in ionic radii; 0.78 Å for Cd^{2+} and 0.66 Å for Mn^{2+}. The formation of Fe_2O_3 is supposed to be as a result of the presence of Mn^{3+} and/or an error in the starting material weights; percentage of the Fe_2O_3 minor phase is changed with the of Mn content. The XRD patterns of PMMA and PMMA/$Cd_{1-x}Mn_xFe_2O_4$ nanocomposites are revealed in Fig. 1b. The figure showed a typical XRD pattern of PMMA with some broad diffraction peaks convoying diffraction lines. The XRD patterns show no difference between pure PMMA and PMMA doped with $Cd_{1-x}Mn_xFe_2O_4$ due to the small percentage of ferrite doping amount. Nevertheless, no diffraction pattern for $Cd_{1-x}Mn_xFe_2O_4$ is a good mark that it is homogeneously dispersed all over the PMMA with no clustering.

3.2 Infrared Spectroscopic Study

Fourier transformation infrared (FTIR) spectra of $Cd_{1-x}Mn_xFe_2O_4$ in PMMA matrix are revealed in Fig. 2. The FTIR spectrum of pure PMMA revealed the functional

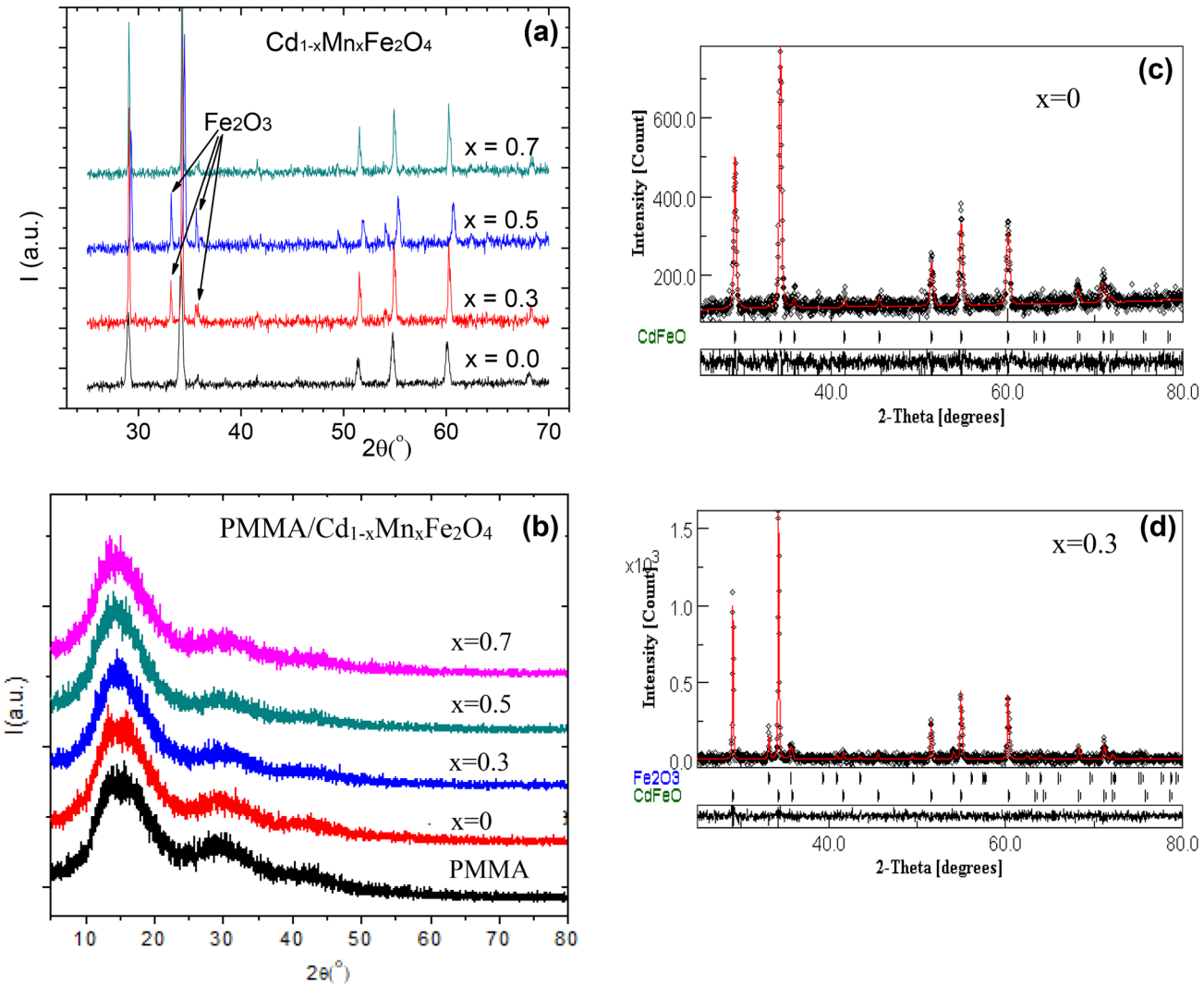

Fig. 1 XRD patterns for **a** nano $Cd_{1-x}Mn_xFe_2O_4$ ferrite and **b** pure PMMA and PMMA loaded with $Cd_{1-x}Mn_xFe_2O_4$ nano ferrite with Rietveld analysis for **c** $CdFe_2O_4$ and **d** $Cd_{0.7}Mn_{0.3}Fe_2O_4$

Table 1 The lattice parameter (*a*), oxygen position (*u*), crystallite size (CS) and the amount of Fe_2O_3 phase obtained from Rietveld refinement for nano $Cd_{1-x}Mn_xFe_2O_4$

x	*a* (Å)	(*u*)O	CS(nm)	Fe_2O_3 %
0	8.708	0.3915	51	0.0
0.3	8.682	0.3909	71	10
0.5	8.632	0.3898	71.5	15
0.7	8.515	0.3797	123	5

groups exist in the pure PMMA. A peak emerged at 1745 cm^{-1} owing to the existence of ester carbonyl group stretching vibration, C=O stretching [23]. The band at 3438 cm^{-1} is belonged to C=O stretching frequency [23]. The peak at 2958 cm^{-1} is ascribed to the existence of stretching vibration of C–H [23]. The peaks ranging from 1000 to 1260 cm^{-1} can be clarified due to the C–O (ester bond) stretching vibration [23]. The peak at 1480 cm^{-1} is assigned to C=C stretching [23]. It is obvious that the peak positions of $Cd_{1-x}Mn_xFe_2O_4$/PMMA are approximately constant for all nanocomposite samples. This could be clarifying as the following: when ferrite doped polymer, ferrites occupied the positions of the voids in the network of the polymeric chains. Consequently, there is no stress of the nano-ferrite on the polymer matrix. The vibrational modes of tetrahedral metal–oxygen and octahedral metal–oxygen [9–11] did not notice in the FTIR spectrum because of the low amount of nano ferrite doped in PMMA matrix.

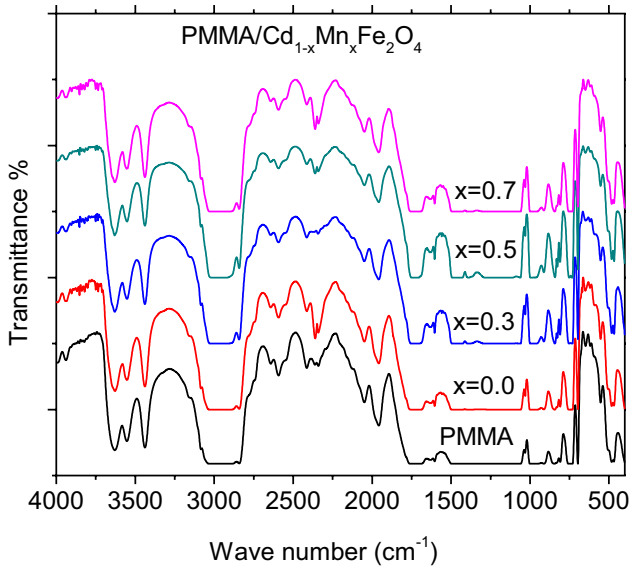

Fig. 2 FTIR for pure PMMA and PMMA loaded with $Cd_{1-x}Mn_xFe_2O_4$ nano ferrite

3.3 UV Spectral and Dispersion Characteristics for PMMA/$Cd_{1-x}Mn_xFe_2O_4$ Nanocomposite

Figure 3 shows the absorbance and transmittance-wavelength dependence for undoped and doped PMMA with $Cd_{1-x}Mn_xFe_2O_4$. As shown in the figure, the absorption peak of PMMA doped nanocomposites has been increased as compared with undoped PMMA sample. On the other hand, it is obvious that transmittance reduced as PMMA loaded with ferrite. A similar effect was observed in ZnSe:Mn/ZnS [18] or $CrCl_2$ [24] or $KMnO_4$ [25] or iron chromate-102 [26] loaded PMMA nanocomposites. This changes either in absorbance or transmittance spectra indicated the existence of a chemical interaction between PMMA and doped ferrite. The rise in the absorption is ascribed to the existence of ferrite in PMMA matrix, which increased the absorbing ability of the nanocomposite matrix. On the other hand, the transmittance of PMMA is the highest among all nanocomposites because it does not have free electrons; electrons are strongly connected to their atoms throughout covalent bonds and the breaking of electron linkage and moving to the conduction band required a photon with high energy. As PMMA polymer loaded with ferrite, part of incident light is absorbed by the substance and does not penetrate through it, thus the transmittance of the nanocomposites is reduced.

The optical energy band gap (E_g) of the nanocomposite films was determined using Tauc's relationship [27]

$$\alpha h\nu = B\left(h\nu - E_g\right)^n$$

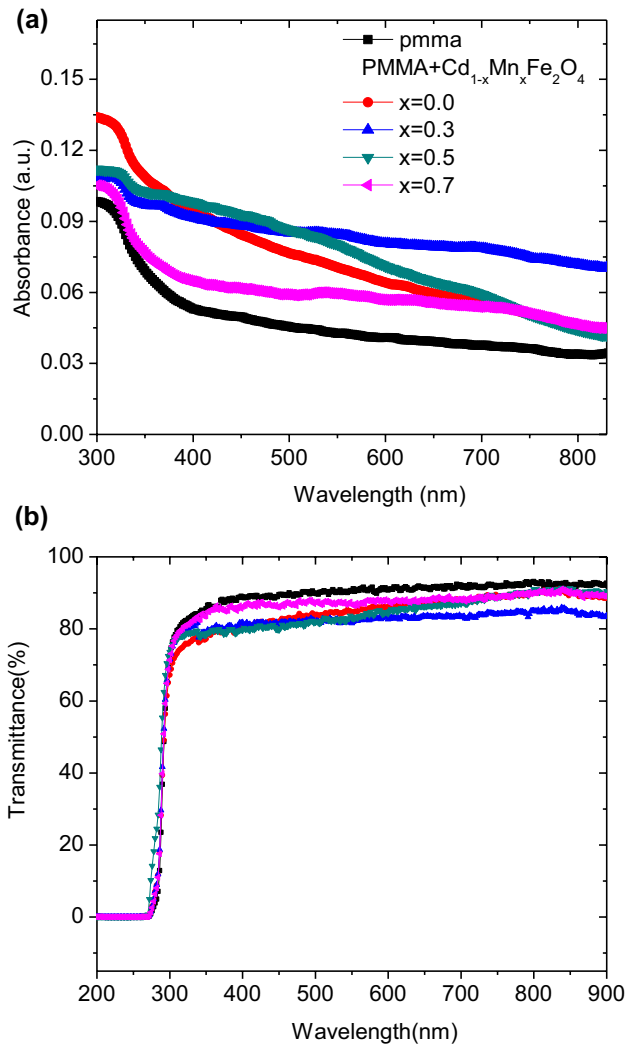

Fig. 3 UV–vis: **a** absorption and **b** transmittance spectra for pure PMMA and PMMA loaded with $Cd_{1-x}Mn_xFe_2O_4$ nano ferrite

where α, B, n and hυ are absorption coefficient, const depends on electronic transition probability, characterize the kind of electronic transition (n = 1/2 or 2 for direct or indirect transition, respectively) and photon energy, respectively.

Figure 4 represents the relation between $(\alpha h\upsilon)^2$ and hυ for PMMA and PMMA loaded with $Cd_{1-x}Mn_xFe_2O_4$. The direct band gap can be evaluated by extrapolating the linear part of the curve $(\alpha h\upsilon)^2$ against hυ to zero absorption value. The calculated band gap values are tabulated in Table 2. From the table the direct energy gap for pure PMMA is 4.56 eV which is larger than the value obtained by Ramli et al. (4.2317 eV) [28] and slightly larger the value got by Elimat et al. (4.5 eV) [29]. As PMMA loaded with ferrite, the energy gap changed, similar effect was observed in carbon nano-tubes/PMMA nanocomposite [30]. Such variation in the value of E_g may be owing to the formation of chemical bonding between PMMA chains and doped ferrite responsible for the generation of localized

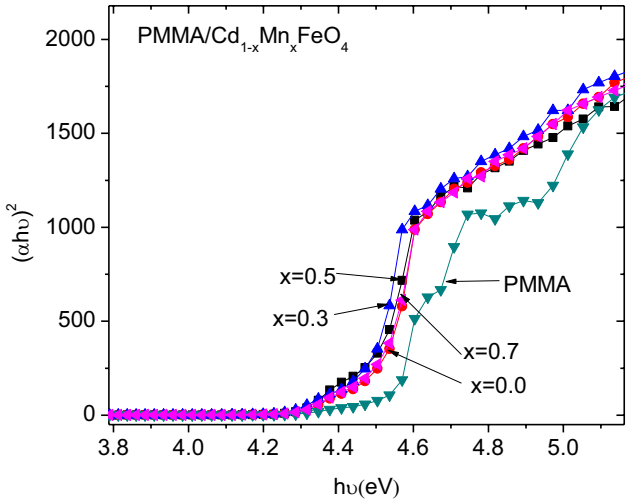

Fig. 4 Plots of $\alpha h\nu)^2$ versus the photon energy (hν) for pure PMMA and PMMA loaded with $Cd_{1-x}Mn_xFe_2O_4$ nano ferrite

states (charge transfer complexes) between the HOMO and LUMO energy bands allowing the lower energy transitions possible which relies on the defects inside the material; as the quantity of Mn-doped increased the crystallite improved and also the quantity of Fe_2O_3 phase altered inside the samples, see XRD part.

The refractive index is a significant parameter which persuades important information for the optical materials and is considered as a complex quantity. The refractive index (n) can be determined by means of the next equations [31]:

$$n = \frac{1+R}{1-R} + \sqrt{\frac{4R}{(1-R)^2} - k^2}$$

$$R = 1 - \sqrt{T * EXP(A)}$$

$$k = \frac{}{2}$$

$$\alpha = \frac{2.303 * \text{absorbance}}{\text{sample thickness}}$$

where R, T, k, α and λ are the reflection, transmission, extinction coefficient, absorption coefficient of the material and the incident light wavelength, respectively. It is obvious from Fig. 5 that the refractive index reduced with increase the wavelength and increased with ferrite doping for all samples. As ferrite incorporated in PMMA matrix the density increased, therefore the refractive index of nanocomposite increased as compared with pure PMMA [30].

According to Wemple and DiDomenico single oscillator model, the dispersion of refractive index below the inter band absorption edge is given as [32]:

$$n^2(h\nu) = 1 + \frac{E_o E_d}{E_o^2 - (h\nu)^2}$$

where E_o is the single oscillator energy that stimulates all electronic excitation involved and E_d is the dispersion energy which is associated with the average strength of the optical transitions. The values of E_d and E_o can be directly evaluated

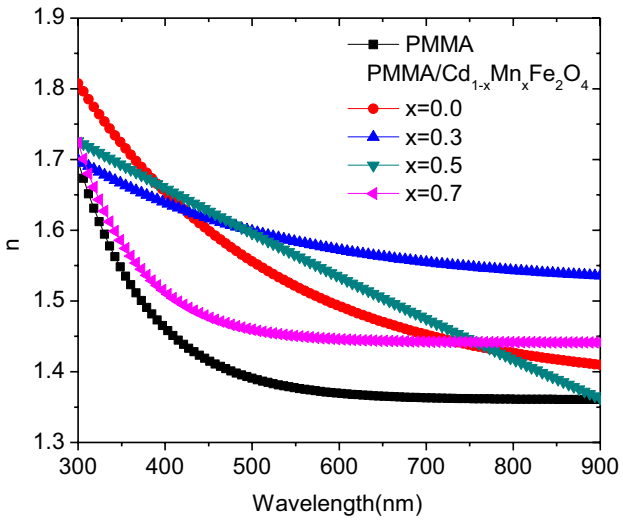

Fig. 5 The dependence of the refractive index (n) on wavelength (λ) for pure PMMA and PMMA loaded with $Cd_{1-x}Mn_xFe_2O_4$ nano ferrite

Table 2 The optical parameters of the all investigated composite films for pure PMMA and PMMA loaded with $Cd_{1-x}Mn_xFe_2O_4$nano ferrite

Sample	E_g (eV)	E_d (eV)	E_o (eV)	f $(eV)^2$	n_o	λ_o (nm)	ε_∞ (eV)	(N/m*) $\times 10^{-51}$ (m^{-3})	S_o $\times$ 10^5 (nm^{-2})
PMMA	4.28	4.78	5.64	26.96	1.34	233.67	1.79	20.5	1.57
PMMA/$Cd_{1-x}Mn_xFe_2O_4$									
x = 0.0	4.3	5.43	5.02	27.26	1.45	239.64	2.11	11.1	1.93
x = 0.3	4.26	10.33	7.46	77.06	1.55	162.63	2.39	35.9	5.27
x = 0.5	4.56	6.11	5.09	31.09	1.54	185.21	2.39	37.6	4.04
x = 0.7	4.31	7.29	7.01	51.10	1.43	169.93	2.05	20.8	3.63

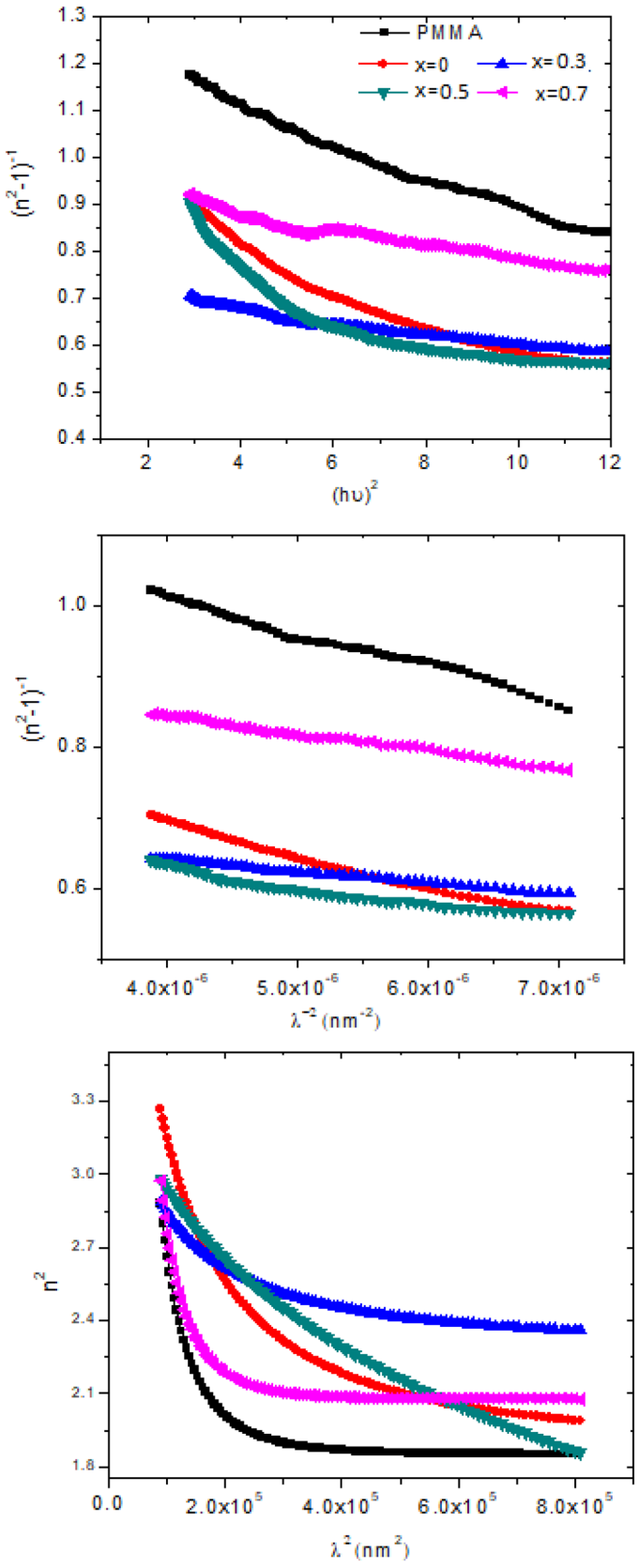

Fig. 6 The variation of **a** $(n^2-1)^{-1}$ versus $(h\nu)^2$, **b** $(n^2-1)^{-1}$ versus λ^{-2}, and **c** n^2 versus λ^2 plots, for pure PMMA and PMMA loaded with $Cd_{1-x}Mn_xFe_2O_4$ nano ferrite

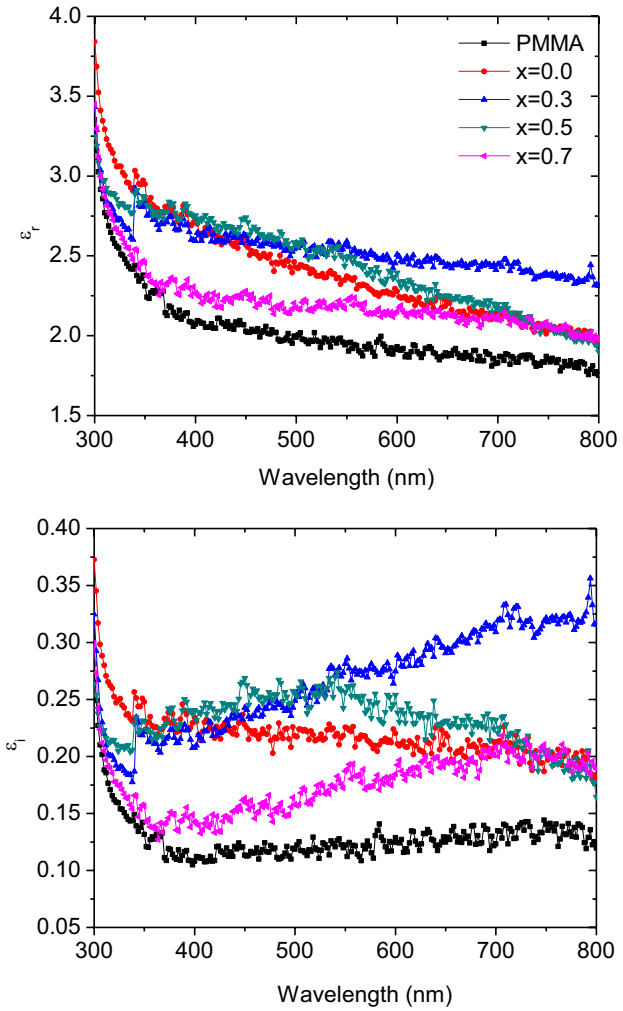

Fig. 7 **a** Real and **b** imaginary parts of the dielectric constant for pure PMMA and PMMA loaded with $Cd_{1-x}Mn_xFe_2O_4$ nano ferrite

from the slope and intercept on the vertical axis of $(n^2-1)^{-1}$ versus $(h\nu)^2$ scheme as revealed in Fig. 6.

The refractive index at zero photon energy (n_o), average inter-band oscillator wavelength (λ_o), the average oscillator strength (S_o), dielectric constant at the infinite wavelength ($\varepsilon_\infty = n_o^2$) and oscillator strength ($f = E_o\, E_d$) can be calculated by means of the single term Sellmeier oscillator [33]:

$$\frac{n_o^2-1}{n^2-1} = 1-\left(\frac{\lambda_o}{\lambda}\right)^2$$

$$\left(n^2-1\right) = \frac{S_o\lambda_o^2}{1-\frac{\lambda^2}{\lambda_0^2}}$$

where

$$S_o = \frac{n_o^2-1}{\lambda_0^2}$$

Figure 6 demonstrates the dependence plot of $(n^2-1)^{-1}$ on λ^{-2} of the films. λ_o and S_o values can be calculated from the slope and intercept of $(n^2-1)^{-1}$ versus λ^{-2} relations, respectively.

The relation between the lattice dielectric constant (ε_L), and the ratio between carrier concentration (N) and the electron effective mass (m^*) which is $\left(\frac{N}{m^*}\right)$, can be estimated according to the following equation [33] by drawing a relation between n^2 and λ^2, Fig. 6,

$$n^2 = \varepsilon_L - \left(\frac{e^2}{c^2}\right)\left(\frac{N}{m^*}\right)^2$$

The values of $\left(\frac{N}{m^*}\right)$ was got from the slope of the linear part of the graph. The obtained values of E_d, E_o, f, S_o, λ_o, ε_∞, n_o and $\left(\frac{N}{m^*}\right)$ are summarized in Table 2. Checking of Table 2 one can notice that all the above parameters changed irregularly due to several factors included the defect and different phases inside the samples, see XDR part. The real and imaginary dielectric constant is defined as:

$$\varepsilon_r = n^2 - k^2 \text{ and } \varepsilon_i = 2nk, \text{ respectively,}$$

where ε_r and ε_i are real and imaginary parts of the dielectric constant. The wavelength dependence values of ε_r and ε_i are shown in Fig. 7 for pure and doped films. The values of ε_r are higher than values of ε_i. Also all doped nanocomposites materials have dielectric larger than pure PMMA owing to the presence of extra density of state (DOS), resulting an enhancement of the polarization that improves the values of dielectric constant [34].

3.4 Photoluminescence (PL) Emission of $Cd_{1-x}Mn_xFe_2O_4$/PMMA Nanocomposites

Figure 8 reveals the photoluminescence (PL) emission for PMMA and $Cd_{1-x}Mn_xFe_2O_4$/PMMA nanocomposites under 250 nm excitation wavelengths which is recognized as a result of the structure defects inside the samples. As noticed from the figure, PMMA emitted four sub emission colors; in UV region (275, 324) nm and visible region (549, 670) nm. Also, all nanocomposite samples emitted four sub emitted colors; two in UV region and two invisible region (green and orange). The UV emissions can be attributed to band to band transition from valence to conduction band [35]. The green emission peak at 533 nm

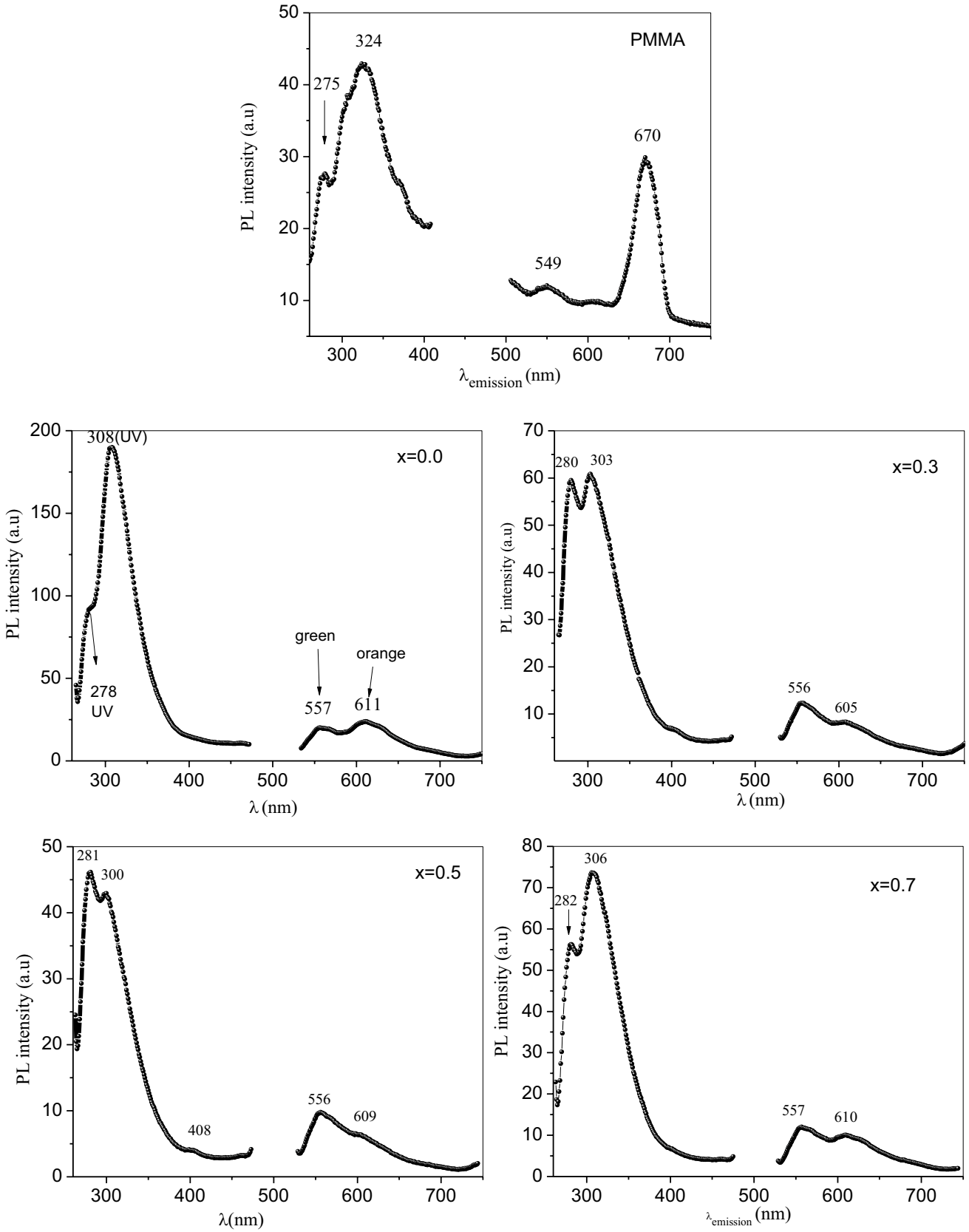

Fig. 8 PL spectra PMMA and $Cd_{1-x}Mn_xFe_2O_4$/PMMA nanocomposites at 250 nm excitation

is as a result of color centers connected to the oxygen vacancies which trapped the excited electron giving rise to F^+ center (with one electron) and F center (with two electrons) [36]. The orange emission may be due to the formation of deep traps levels inside the band gap [37]. Moreover, the PL intensities of all nanocomposite materials have been enhanced upon doping PMMA with ferrite. A similar trend was observed previously in CdSe/PMMA [35], but the UV intensity quenched while visible emission was enhanced upon CdSe doped ratio increased. This result is in contrary to our case where the intensity exhibited an irregular trend due to the existence of the above different factors; $Cd_{1-x}Mn_xFe_2O_4$/PMMA nanocomposite exhibited the highest PL intensity while $Cd_{1-x}Mn_xFe_2O_4$/PMMA nanocomposite showed the lowest one.

4 Conclusion

Fourier transformation infrared showed the characteristics bands for PMMA and the band positions of $Cd_{1-x}Mn_xFe_2O_4$/PMMA are approximately constant for all nanocomposite samples. UV analysis revealed that absorbance was enhanced while transmittance was reduced as PMMA loaded with nano ferrite. The direct energy gap for pure PMMA is 4.56 eV and as PMMA loaded with ferrite it changed depending on the defects present inside the material. The refractive index increased as ferrite incorporated in PMMA matrix due to the increase of the density. All optical parameters changed irregularly due to defects and the present of Fe_2O_3 phase inside the doped ferrite samples. All doped nanocomposites materials have dielectric larger than pure PMMA. Photoluminescence investigation revealed that $Cd_{1-x}Mn_xFe_2O_4$/PMMA nanocomposites have emitted four sub-emitted colors; in UV and visible regions (green and orange) depend on the location of the defect in the band gap of the material.

Acknowledgements The authors are grateful to the Deanship of Scientific Research, King Saud University for funding through Vice Deanship of Scientific Research Chairs.

References

1. A. Ehsani, M. Bigdeloo, M.Y. Ansari, B. Mirtamizdoust, A.A. Heidari, M. Hadi, H.M. Shiri, Bull. Chem. Soc. Jpn. **91**(4), 617 (2018)
2. G. Zhao, X. Huang, Z. Tang, Q. Huang, F. Niu, X. Wang, Polym. Chem. **9**, 3562 (2018)
3. S. Botsi, C. Tsamis, M. Chatzichristidi, G. Papageorgiou, E. Makarona, Nano-Struct. Nano-Objects **17**, 7 (2019)
4. X. Huang, R. Wang, T. Jiao, G. Zou, F. Zhan, J. Yin, L. Zhang, J. Zhou, Q. Peng, ACS Omega **4**, 1897 (2019)
5. H. Zhu, K.C. Jha, R.S. Bhatta, M. Tsige, A. Dhinojwala, Langmuir **30**, 11609 (2014)
6. A. Sharma, R.K. Karn, S.K. Pandiyan, A. Sharma, R.K. Karn, S.K. Pandiyan, J. Basic Appl. Eng. Res. **1**, 1 (2014)
7. M. Nandimath, R.F. Bhajantri, J. Naik, V. Hebbar, J. Lumin. **207**, 571 (2019)
8. Z.K. Heiba, M.B. Mohamed, Appl Phys A **124**(12), 818 (2018)
9. K. El-Sayed, M.B. Mohamed, S. Hamdy, S.S. Ata-Allah, J. Magn. Magn. Mater. **423**, 291 (2017)
10. Z.K. Heiba, M.B. Mohamed, J. Mater. Sci.: Mater. Electron. **30**(1), 786 (2019)
11. Z.K. Heiba, N.G. Imam, M.B. Mohamed, J. Mol. Struct. **1095**, 61 (2015)
12. H. Yang, Y. Zhuang, H. Hu, X. Du, C. Zhang, X. Shi, H. Wu, S. Yang, Adv. Funct. Matter **20**, 1733 (2010)
13. V. Nagarajan, A. Thayumanavan, Appl. Surf. Sci. **428**, 748 (2018)
14. S.B. Patil, H.S.B. Naik, G. Nagaraju, Y. Shiralgi, Eur. Phys. J. Plus **133**(6), 229 (2018)
15. X. Zhou, Y. Zhou, L. Zhou, J. Wei, J. Wu, D.Yao, Ceram. Int. **45**(5), 6236 (2019)
16. R. Bisen, J. Tripathi, A. Sharma, A. Khare, Y. Kumar, S. Tripathi, Vacuum **152**, 65 (2018)
17. S. Khursheed, P. Biswas, V.K. Singh, V. Kumar, H.C. Swart, J. Sharma, Vacuum **159**, 414 (2019)
18. K.M. Postolek, K.C. Gorka, M. Bredol, K. Guguła, J. Lumin. **203**, 655 (2018)
19. J. Bai, Y. Liu, Y. Hou, S. Wang, Mater. Chem. Phys. **217**, 486 (2018)
20. D. Padalia, U.C. Johri, M.G.H. Zaidi, Physica B **407**(5), 838 (2012)
21. D. Ding, X. Yan, X. Zhang, Q. He, B. Qiu, D. Jiang, H. Wei, J. Guo, A. Umar, L. Sun, Q. Wang, M.A. Khan, D.P. Young, X. Zhang, B. Weeks, T.C. Ho, Z. Guo, S. Wei, Superlattices Microstruct. **85**, 305 (2015)
22. L. Lutterotti, Maud 2.33, http://www.ing.unitn.it/~maud/
23. A.K. Kushwaha, N. Gupta, M.C. Chattopadhyaya, Arab. J. Chem. **10**(2), S1645 (2017)
24. K. Al-Ammar, A. Hashim, M. Husaien, Chem. Mater. Eng. **1**, 85 (2013)
25. A.K. Gupta, M. Bafna, Y.K. Vijay, Bull. Mater. Sci. **41**, 160 (2018)
26. B.R. Ali, F.N. Kadhem, Int. J. Appl. Innov. Eng. Manag. **2**, 114 (2013)
27. J. Tauc, in A. Abeles (ed.), The Optical Properties of Solid (North Holland, Amsterdam, 1972), p. 277
28. Z.H. Ramli, N.F.A. Zainal, M. Rusop, AIP Conf. Proc. **1136**, 761 (2009)
29. Z.M. Elimat, A.M. Zihlif, M. Avella, J. Exp. Nanosci. **3**(4), 259 (2008)
30. Z.K. Heiba, M.B. Mohamed, N.G. Imam, J. Inorg. Organomet. Polym Mater. **26**(4), 780 (2016)
31. N.F. Mott, E.A. Davis, *Electronic Processes in Non-crystalline Materials* (Clarendon Press, Oxford, 1979)
32. S.H. Wemple, Di Domenico, Phys. Rev. B **3**, 1338 (1971)
33. S.H. Wemple, M. DiDomenico Jr., Phys. Rev. B **2**(3), 1338 (1971)
34. Z.K. Heiba, M.B. Mohamed, J. Mol. Struct. **1181**, 321507 (2019)
35. Z.K. Heiba, M.B. Mohamed, N.G. Imam, J. Mol. Struct. **1136**, 321 (2017)
36. B. Choudhury, B. Borah, A. Choudhury, Photochem. Photobiol. **88**, 257 (2012)
37. M.B. Mohamed, Z.K. Heiba, N.G. Imam, J. Mol. Struct. **1163**, 442 (2018)